The Influence of Floating Turbine Dynamics on the Helix Wake Mixing Method

van den Berg, D.G.; De Tavernier, Delphine; Gutknecht, Jonas; Viré, Axelle; Van Wingerden, Jan Willem

DOI
10.1088/1742-6596/2767/3/032012

Publication date
2024

Document Version
Final published version

Published in
Journal of Physics: Conference Series

The Influence of Floating Turbine Dynamics on the Helix Wake Mixing Method

Journal of Physics: Conference Series **2767** (2024) 032012 doi:10.1088/1742-6596/2767/3/032012

The Influence of Floating Turbine Dynamics on the Helix Wake Mixing Method

Daniel van den Berg[1], Delphine de Tavernier[2], Jonas Gutknecht[1], Axelle Viré[2] and Jan-Willem van Wingerden[1]

[1]Delft Center for Systems and Control, Delft University of Technology, Mekelweg 2, 2628 CD Delft, The Netherlands
[2]Wind Energy Section, Delft University of Technology, Kluyverweg 1, 2629 HS Delft, The Netherlands.

E-mail: d.g.vandenberg@tudelft.nl

Abstract. Wake mixing techniques like the Helix have shown to be effective at reducing the wake interaction between turbines, which improves wind farm power production. When these techniques are applied to a floating turbine it will excite movement. The type and magnitude of movement are dependent on floater dynamics. This work investigates four different floating turbines. Of these four turbines, two are optimised variants of the TripleSpar and Softwind platforms with enhanced yaw motion. The other two are the unaltered versions of these platforms. When the Helix is applied to all four floating turbines, the increased yaw motion of the optimised TripleSpar results in a reduction in windspeed whereas the optimised Softwind sees an increase in windspeed with increased yaw motion. From simulations using prescribed yaw motion at different phase offsets between blade pitch and yaw motion, we can conclude that this is the driving factor for this difference.

1. Introduction

The floating wind market is rapidly growing, with Europe aiming to have 4 GW of installed capacity operational by 2030. This is a substantial increase from the currently operational 0.18 GW installed capacity [1]. Unlike its bottom-fixed counterpart, there is not yet a convergence on the 'optimal' design of a floating wind turbine. Currently, more than 50 different types of substructures for floating turbines are being developed in academia and industry alike [2]. Regardless of floater design one of the main challenges for floating wind is the interaction between conventional wind turbine control and the dynamics of the floating platform [3].

One area where the interaction with the floater dynamics can provide benefits is wind farm flow control. Within a wind farm, the wake interaction between turbines is a major cause of energy loss [4]. For conventional bottom-fixed wind farms, three different control techniques are actively researched that can mitigate this wake interaction, namely wake steering, axial induction control and dynamic pitch control. Over the past decade especially wake steering has been extensively researched and its potential has been proven over a large number of publications covering simulations, wind tunnel experiments and field tests [5, 6, 7].

Wake steering is also one example where the extra degrees of freedom of a floating turbine can be leveraged. In [8] wake deflection is achieved by pitching the floater backwards or forwards. Similarly to wake steering on a bottom-fixed turbine, the misalignment due to the platform

pitch creates a force component that deflects the wake upwards when pitched backwards and downwards when pitched forwards. One of the main findings in [8] is that deflecting the wake downwards towards the ocean surface allows the flow in the free stream from above the turbine to enter the wake which ultimately increases the downstream wind speed.

An alternative solution to wake steering is dynamic wind farm flow control. Two notable methods that fall into this category are dynamic induction control [9] and dynamic individual pitch control (often referred to as 'the Helix' method) [10]. Both techniques use the blade pitch degree of freedom to dynamically vary the magnitude or the location of the thrust vector of the upstream turbine. The time-varying behaviour of the turbine's thrust leads to a time-varying wind speed within the wake which, when excited at the right frequency, can promote the onset of wake mixing.

When these techniques are applied to a floating turbine, the time-varying force will excite movement. The magnitude and phase of the movement with respect to the blade pitch input is heavily dependent on the type of floater on which the turbine is mounted. For example, the Helix wake mixing method applies a time-varying tilt and yaw moment to the turbine that typically is of such magnitude that the motions remain small. However, semi-submersible type floaters such as the TripleSpar [11] have an eigenfrequency in yaw motion for which the excitation frequency falls within the frequency range with which the Helix is typically applied [12, 13]. For a typical blade pitch input used for the Helix wake mixing method the resulting yaw motion can reach between 5 to 10 degrees for these type of platforms.

The influence that the yaw motion has on the Helix and the onset of wake mixing was first investigated in [12]. In that work prescribed motion was used to replicate the floating turbine motion. An increase in downstream wind speeds was observed when the turbine was yawing. The same interaction is investigated in [13] and did not use prescribed motion but rather simulated the full coupling. In [13] it was found that actuating at the eigenfrequency, which leads to the largest yaw excursions, diminished the effectiveness of the Helix wake mixing method.

This work aims to provide an answer to the question of why actuating the Helix method at the eigenfrequency of a floating turbine can lead to reduced effectiveness of the Helix method. For this purpose, the contribution of this paper is twofold: (1) It provides an analysis of the movement that a turbine undergoes near and at the eigenfrequency using a frequency domain analysis and, (2), it investigates wake recovery behind the floating turbines using time-domain simulations. The remainder of this paper is organised as follows. Section 2 introduces the research methodology and describes the two floating turbines used in this work. Sections 3 and 4 show and explain the frequency and time-domain results, respectively. Finally, Section 5 forms the conclusion of this work.

2. Methodology

In this work, QBlade [14] is used to conduct all investigations. QBlade can simulate the aero, structural and hydrodynamics of a floating turbine within a single simulation environment. The hydrodynamic solver in QBlade has extensively been verified against other simulation suites [15]. Within QBlade the wake aerodynamics are modelled using a free wake vortex method. Although such a modelling technique typically loses accuracy when wake breakdown has occurred it can be used to predict the breakdown location accurately [16]. Knowing the location of the breakdown provides insight into when the wake mixing process is triggered. QBlade has previously been used in [12, 17, 13] for a similar type of research. The settings described in [17] are also used in this work.

All simulations are carried out using the DTU 10MW [18] mounted on the TripleSpar [11] and Softwind [19] platforms. Both turbines are shown in Figure 1a. The TripleSpar is a semi-submersible type of platform while the Softwind is a spar-buoy type. Two other floating turbines are also included in the simulations. These turbines are optimised versions of the TripleSpar and

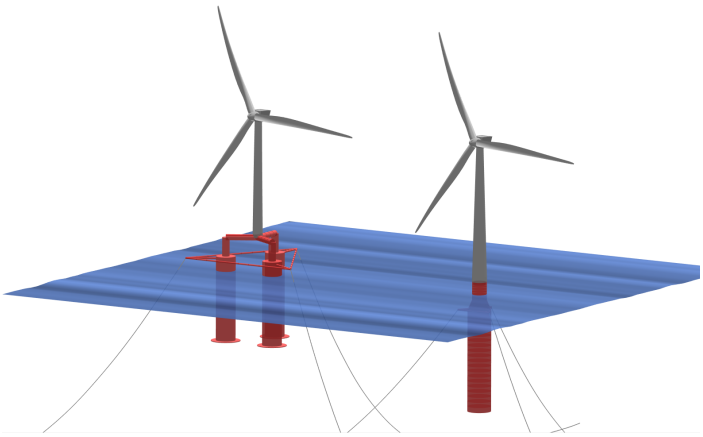

(a) TripleSpar (left) and Softwind (right).

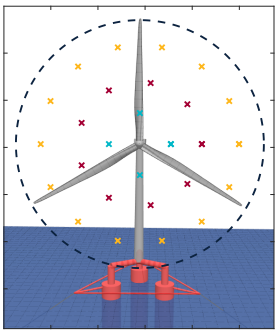

(b) Measurement Points for analysis.

Figure 1: Figure 1a: A screenshot taken in QBlade showing both the TripleSpar (left) and Softwind (right) floater supporting a DTU 10MW turbine. Figure 1b: Measurement points used for analysis overlayed on the DTU 10MW turbine.

Softwind and have enhanced yaw motion when the Helix method is applied. The optimization was part of the FLOATECH project and the details of the optimization set-up can be read in [20]. Because the movement of the floating turbine is frequency-dependent, the Helix will be applied at different actuation frequencies. We make the actuation frequency dependent on turbine size, wind speed and desired Strouhal number. The Strouhal number is a non-dimensionalised frequency which is defined as

$$S_t = \frac{V_\infty f_e}{D}, \tag{1}$$

in which V_∞ is the free stream velocity in [m/s], f_e is the blade pitch frequency in [Hz] and D is the rotor diameter in [m]. The following input frequencies are used:

$$S_t = \begin{bmatrix} 0 & 0.10 & 0.15 & 0.20 & 0.25 & 0.30 & 0.35 & 0.40 & 0.45 & 0.50 & 0.60 & 0.70 \end{bmatrix}, \tag{2}$$

in which $S_t = 0$ represents a baseline case without any pitch actuation. Although it is still a topic of ongoing research, currently it is believed that the range from $S_t = 0.30$ to $S_t = 0.40$ is ideal for the Helix in terms of promoting wake recovery [21, 22]. For all simulations, the amplitude of the blade pitch angle is set to 4 degrees. The wind speed in the wake is calculated by taking 27 independent measurements at points distributed over the rotor disk of a hypothetical downstream turbine. The distribution of the points can be seen in Figure 1b.

Wind speed measurements are taken at the following downstream distances, defined in terms of rotor diameter,

$$D = \begin{bmatrix} -1.0 & 0.0 & 1.0 & 2.0 & 2.5 & 3.0 & 3.5 & 4.0 & 4.5 & 5.0 & 6.0 \end{bmatrix}. \tag{3}$$

The length of the domain is limited to $6D$ because the free vortex wake method loses accuracy when wake breakdown occurs and the mixing process starts. In total 12 different actuation frequencies are evaluated for which the wind speed is measured at 11 different distances. The simulations are performed in batches using MATLAB running QBlade through a Dynamic-Link Library interface to streamline the simulation process [23].

For all simulations, the same environmental conditions are used. The inflow speed is set to 9 m/s and is considered uniform. This is an idealization of a real-world scenario as the mixing effect introduced by the Helix is more pronounced without any natural mixing coming from turbulence. Nevertheless, the Helix remains effective in turbulent conditions. The work done in [24] and [25] both used a turbulence level of 5% and found accelerated recovery when the Helix was applied. Furthermore, the wave conditions used are based on the IEC 61400-3-1:2019 standard which specifies the type of wave field to use for different wind conditions [26]. The size and frequency content of the waves are characterised using a JONSWAP wave spectrum [27].

3. Floating Turbine Dynamics

The Helix can be applied by setting a time-varying signal on the fixed-frame pitch signals β_{tilt} and β_{yaw}. These signals can be transformed into individual pitch signals using the MBC transformation [28]. The resulting time-varying individual pitch angles create time-varying out-of-plane bending moments for the individual blades. These can be transformed into fixed-frame moments using the MBC transformation, i.e.,

$$\begin{bmatrix} M_{col}(t) \\ M_{tilt}(t) \\ M_{yaw}(t) \end{bmatrix} = \frac{2}{3} \begin{bmatrix} 0.5 & 0.5 & 0.5 \\ \cos(\psi_1(t)) & \cos(\psi_2(t)) & \cos(\psi_3(t)) \\ \sin(\psi_1(t)) & \sin(\psi_2(t)) & \sin(\psi_3(t)) \end{bmatrix} \begin{bmatrix} M_{y,1}(t) \\ M_{y,2}(t) \\ M_{y,3}(t) \end{bmatrix}, \tag{4}$$

In Eq. (4) $M_{y,i}$, with $i \in [1, 2, 3]$, are the individual out-of-plane blade root moments and M_{col}, M_{tilt} and M_{yaw} are the fixed-frame moments. The subscript *col* refers to the collective moment of the turbine. The time-varying fixed-frame β_{tilt} and β_{yaw} pitch angles create time-varying M_{tilt} and M_{yaw} moments. The changing moments will excite movement in a floating turbine. A frequency identification experiment is run for both the original and optimised designs to capture the interaction between the Helix and both floating turbines used in this work. The input for identification is a chirp signal applied to the β_{yaw} channel which excites the system between $1 \cdot 10^{-3}$ and 1 Hz. Based on the measured input-output relations in each degree of freedom, transfer functions can be identified [29].

The results of the identification process are shown in Figure 2. The top row of plots shows the gains from blade pitch input to one of the six degrees of freedom and the bottom row shows the corresponding phase difference between the input and output signal. The left two-by-two block of plots shows the responses in translational motions, that is surge, sway and heave and the right two-by-two block the rotational motions, i.e., roll, platform pitch and yaw. The solid lines are the response functions for the unaltered floating turbines, the dash-dotted line are the response functions of the optimised floating turbines. The translational motions remain relatively small when the system is excited over the fixed-frame yaw axis. The displacement will be at most a few metres for a typical input of two to four degrees of blade pitch which, compared to the turbine size, can be considered small. This is mainly because the collective moment remains near constant and only the fixed frame yaw and tilt axis are excited.

For the rotational motions, the yaw degree of freedom is dominant for both versions of the TripleSpar platform. The difference between the unoptimised and optimised versions is a small shift in the eigenfrequency coupled with an increase in the gain. When the optimization was carried out the optimal mixing frequency was still considered to be $S_t = 0.25$, hence the shift in the location of the eigenfrequency. The unoptimised Softwind floating turbine is relatively insensitive to the input of the Helix. The optimised version, however, has a significantly increased response in yaw. The other two rotational degrees of freedom are much more subdued, except for roll which has an eigenfrequency outside the frequency range typically considered for the Helix. It is unlikely that the presence of waves will impact the motions induced by the Helix as waves excite the system at a different frequency range, typically around 0.1 Hz.

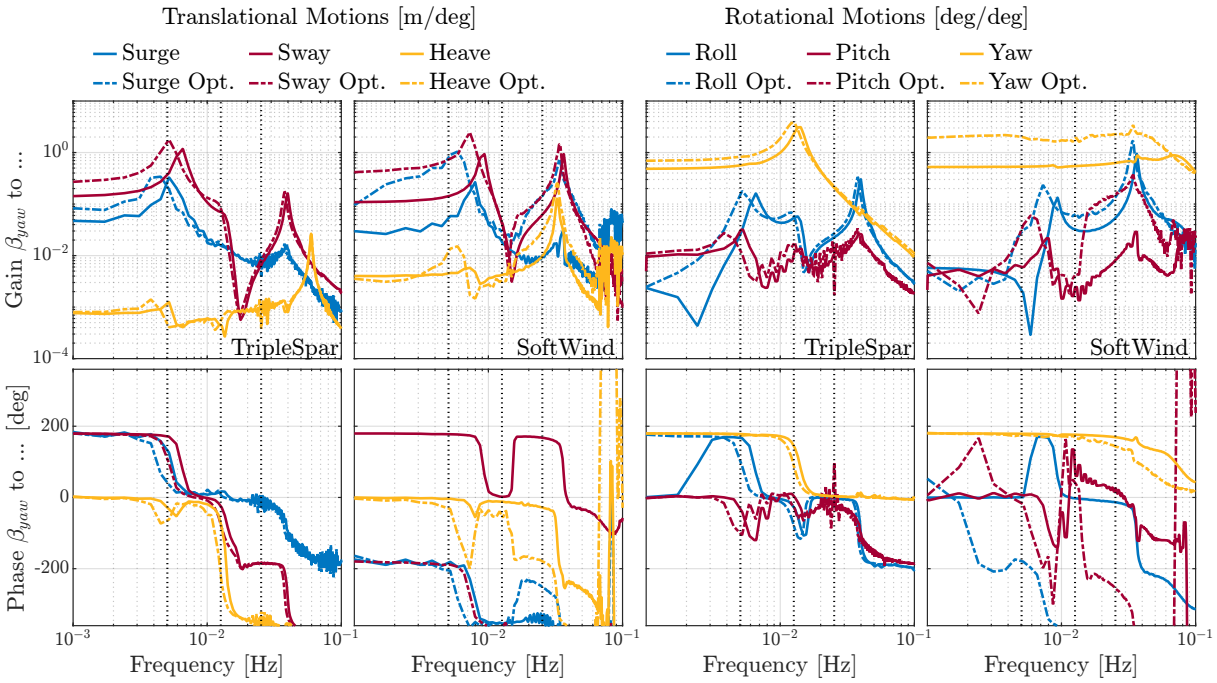

Figure 2: Results from the frequency identification experiments. The 2-by-2 plots on the left contain the response for the translational degrees of freedom for both the TripleSpar and Softwind platforms. The solid line is the response for the original platform design and the dash-dotted line is for the optimised version. The right 2-by-2 plots show the results for the rotational degrees of freedom. The bottom row of the plots shows the phase coupling between the input and output signal. The vertical dashed lines in each plot indicate the frequency corresponding to $S_t = 0.10$, $S_t = 0.25$ and $S_t = 0.50$ for the DTU 10MW turbine.

When the Helix is applied at the eigenfrequency of the optimised TripleSpar platform, both the latter and the optimised Softwind floating turbine will exhibit a comparable magnitude of yaw motion. A big difference, however, is the phase coupling between the blade pitch input and the yaw motion of the turbine. While for the Softwind platform this coupling remains relatively constant within the frequency range of the Helix, for the TripleSpar platform the phase can differ by 180 degrees due to the presence of the eigenfrequency.

A schematic representation depicting how yaw motion can influence the Helix is given in Figure 3. The top row of Figure 3 is a front view of the rotor with the red arrows depicting the patch of the thrust vector when the Helix is applied in a counter-clockwise manner [10]. The blue dot denotes the exact location of the thrust vector at four different time instances within a single Helix period, denoted by T_p. The bottom row shows yaw motion corresponding to 90° phase offset. The blue arrow represents the thrust force.

When the floating turbine is yawing, one-half of the turbine is moving into the flow and one-half is moving out of the flow increasing and decreasing the effective wind speed respectively. Given the phase difference in Figure 3, the thrust vector is located at the side which is moving into the wind. Due to the increased effective windspeed, the thrust is also increased which would increase the yaw moment. The opposite can also hold which would lead to a reduction of the yaw moment. Furthermore, something that is not taken into account in this analysis is the effect of yawing on the wake. To see how this and the change in yaw motion can impact the onset of wake mixing, time-domain simulations are required to analyse the wind speed behind the turbine.

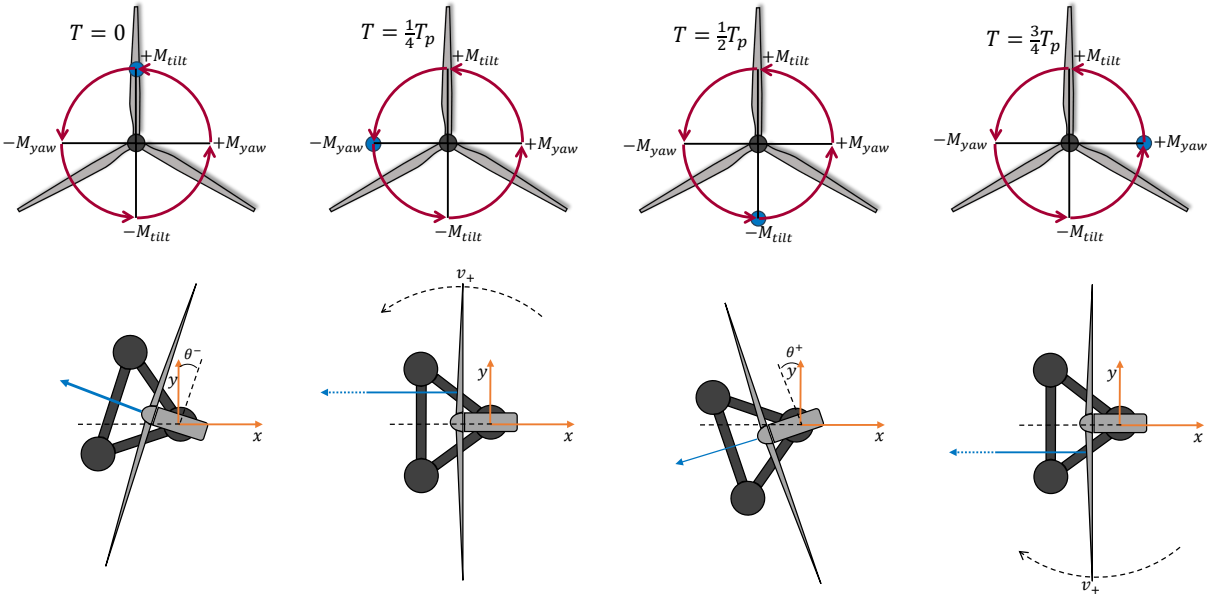

Figure 3: Schematic representation of the Helix and corresponding yaw motion of the floating turbine. The blue dot (top row) and arrow (bottom row) indicates the location of the thrust force of the turbine during a period of the turbine.

4. Wind Speed Results

In this section the wind speed behind the four different floating turbines is investigated with the Helix applied at the frequencies mentioned in Eq. (2). Furthermore, a more synthetic simulation is also carried out. Here the Helix is applied to a bottom-fixed turbine which is yawed with prescribed motion at different phase offsets, defined with respect to the β_{yaw} input. For this simulation a single actuation frequency is chosen, close to the eigenfrequency of the TripleSpar. It will be compared to a case without yawing motion, i.e., the Helix applied to a bottom-fixed turbine and a case without the Helix which serves as a baseline.

4.1. Time Domain Results TripleSpar and Softwind

Figure 4 shows the wind speed data gathered from the simulations. The results are normalised with respect to the inflow velocity $V_\infty = 9$ m/s. The left column shows the results for baseline and optimised TripleSpar and the right column for the Softwind. The largest recovery in wind speed is found for the Strouhal range of $0.20 - 0.40$. This is in line with previous research and it remains largely unaffected by the yawing motion.

When comparing the results between the unoptimised and optimised floaters an interesting difference can be seen between the TripleSpar and Softwind turbines. For the optimised TripleSpar the wind speed is decreased with downstream distance compared to the unoptimised version. For example, for the unoptimised version, the wind speed has recovered to 80% of the inflow at $4.5D$, which has moved to $5.5D$ for the optimised version. For the Softwind this 80% mark moves slightly forward. Furthermore, the frequency range over which this gain in wind speed can be achieved is widened.

The impact of the increased yaw motion is more noticeable when comparing the total power production of a hypothetical two-turbine wind farm. Dynamic yawing will impact the power production of the upstream turbine so it could be that a reduction in power production for the

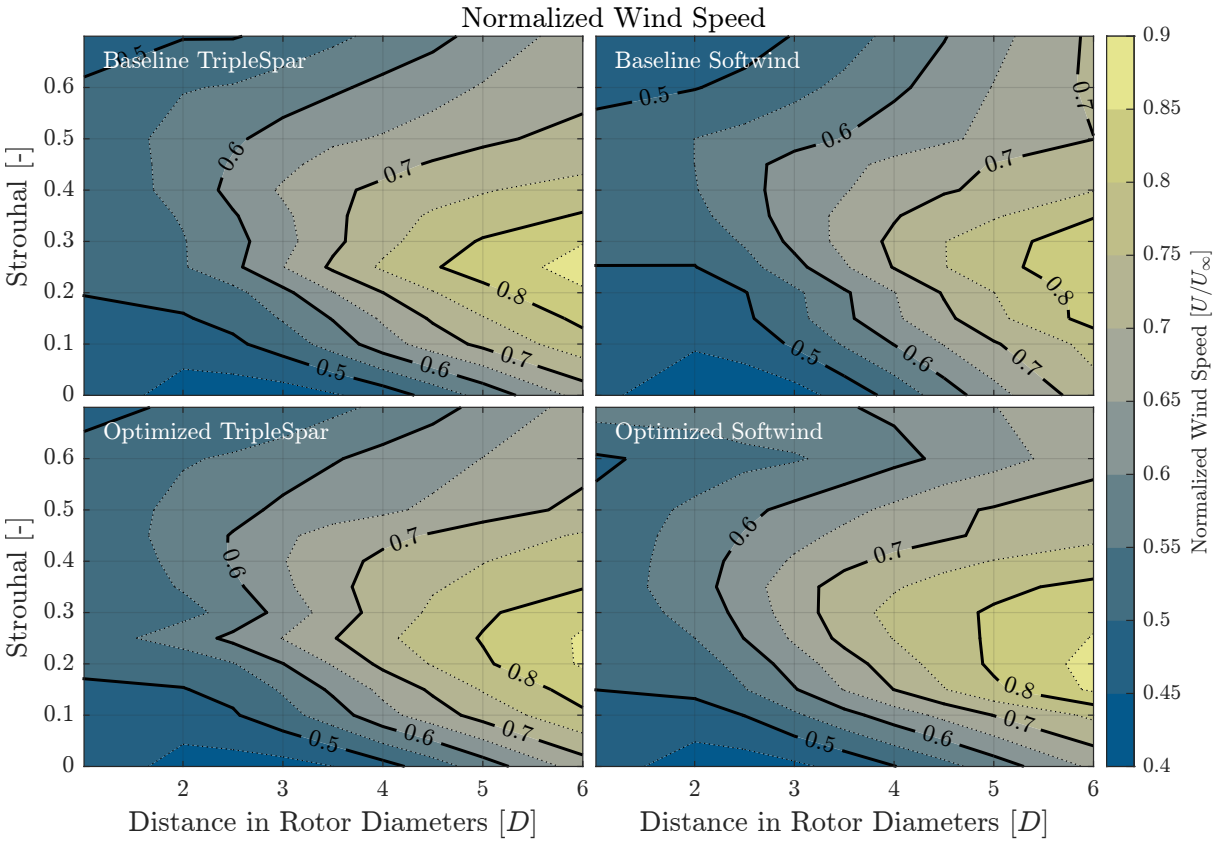

Figure 4: Normalised wind speed behind the four different floating turbines for different actuation frequencies.

first turbine negates the gain in potential power due to increased wind speeds.

Figure 5 shows the relative power production for the wind farm. Based on the measured wind speed the power production for the second turbine is calculated. A relative comparison is made for the power production of a wind farm using the unoptimised floating turbine. A value larger than 1 indicates that the wind farm using the optimised turbine has increased power production. For the TripleSpar there is no major difference in power production. This is mainly because the dynamics are similar between the two floating turbines. However, at the optimization frequency of $S_t = 0.25$, there is a distinct area of reduced power production of which the frequency spans the same range in which the platform will undergo yaw motion when excited by the Helix. For the Softwind turbine, there is a significant increase in power production, up to an increase of 8%. For the Softwind the increased yaw motion contributes positively to the overall wind farm power production.

4.2. Results for Prescribed Yaw Motion

The results obtained using prescribed motion, shown in Figure 6 can clarify this difference between the two floating turbines. The yaw motion is prescribed with an amplitude of 6 degrees and the Helix with 2 degrees of blade pitch. Both the Helix and yaw motion are applied at the same frequency. In total four different phase offsets, varying by 90°, are analysed and compared to the Helix without yaw motion and a baseline case without the Helix and yaw motion. Finally, a case with only yaw motion (i.e. dynamic yaw) is also included in the data. At a phase offset of 180° wind speed is increased behind the turbine compared to the Helix whereas with an offset

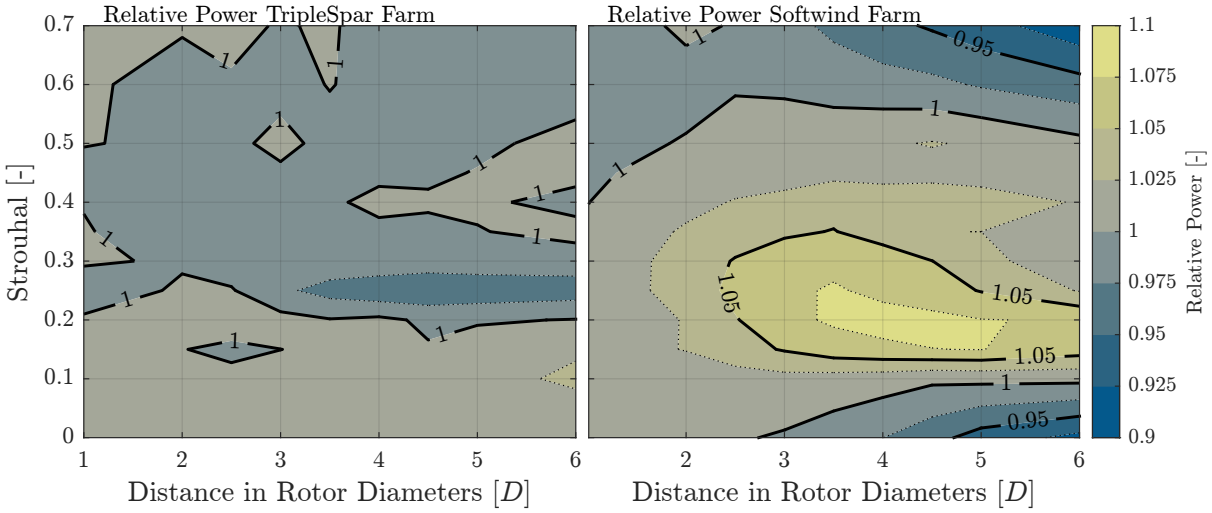

Figure 5: Relative power production of a hypothetical aligned two-turbine wind farm. The total power of the farm is based on the power production of the first turbine and hypothetical power based on the measured wind speed. The power production of the wind farm with the optimised turbine is divided by that of the baseline wind farm. A value of 1 or larger indicates an increase in power production.

of 0° and 270°, there is no difference in wind speed. This confirms that actuating at the right phase coupling can have a positive impact on the performance of the Helix. Furthermore, the difference in windspeed between different phase offsets implies that the dynamic yawing motion interacts with and impacts the wake mixing dynamics of the Helix method. If the yawing motion is only responsible for deflecting the wake then there should be no discernible difference in the downstream wind speed between different phase offsets. Furthermore, adding the gain of dynamic yaw with that of the Helix does not equal one of the cases with both yaw and the Helix implying that their contribution is not a linear combination.

5. Conclusion

This work investigates how the dynamics of a floating turbine interacts with the Helix wake mixing method. Two optimised and unoptimised floating turbines are used in this analysis, where the optimised versions of the floating turbine have enhanced yaw motion. For the TripleSpar, yaw motion is excited by applying the Helix at its eigenfrequency. A consequence of actuating near the eigenfrequency is a potential change of 180° in-phase coupling between the Helix blade pitch input and the yaw motion of the floating turbine. This will influence the moments that are applied to the turbine as well as the deflection of the wake. This is not the case for the Softwind platform. Its optimised version also has increased yaw motion, but the phase coupling remains constant. The interaction with wake mixing is quantified by measuring the wind speed behind the floating turbine. When comparing the optimised TripleSpar with its unoptimised version, a decrease is observed in the wind speed in the wake which implies that the yaw motion negates part of the wake mixing. This is also seen in the relative wind farm power, which shows a distinct area of lower power production centred around the eigenfrequency. However, the opposite is found for the Softwind platform: an increase in yaw motion goes together with an increase in wind speed and power production. Further analysis using prescribed yaw motion confirms that a 180° shift in phase coupling can be the difference between outperforming or underperforming with respect to the Helix without any yaw motion.

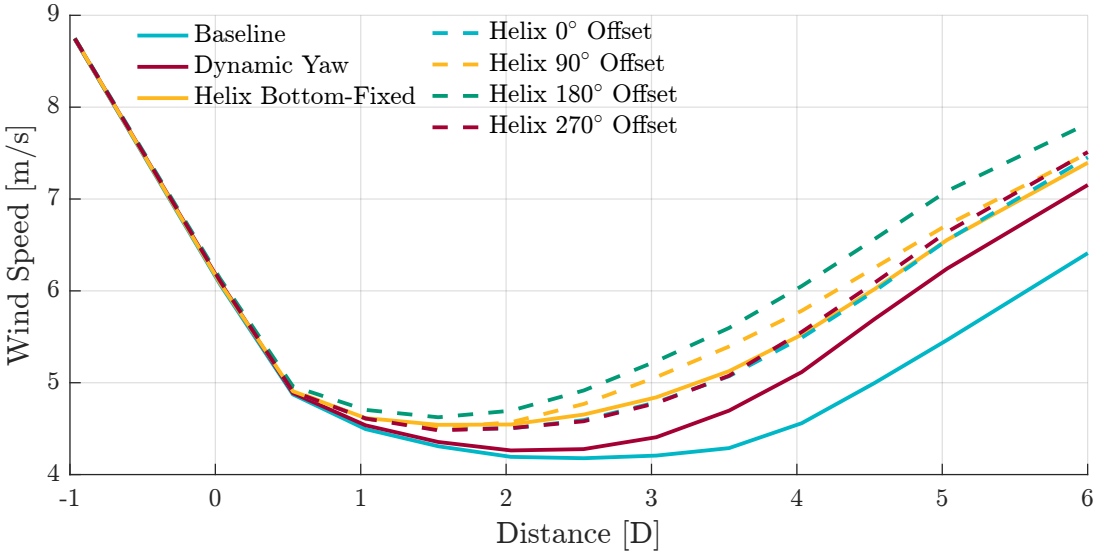

Figure 6: Wind speed analysis using prescribed motion on a bottom-fixed turbine with the Helix at a single frequency. This data has been obtained using the IEA 15MW [30] turbine as results for that turbine were easier to analyse. Whether the interaction between the Helix and yaw motion is diameter-dependent is still an open question.

6. Acknowledgement

This project is part of the Floatech project. The research presented in this paper has received funding from the European Union's Horizon 2020 research and innovation programme under grant agreement No. 101007142.

This project is also part of the Floatfarm project. The research presented in this paper has received funding from the European Union's Horizon.2.5 Climate, Energy and Mobility programme under grant agreement No. 101136091.

7. Data Availability

The data used in this work are available at the 4TU repository [31].

References

[1] "Floating wind is making great strides. *Published: 12-May-2023.*" https://windeurope.org/newsroom/news/floating-wind-is-making-great-strides/, 2023.

[2] Aegir. Insights, "Floating wind foundations: Out of more than 50, which concepts will dominate the market? *Last Accessed: 04-July-2023.*" https://www.aegirinsights.com/floating-wind-foundations-out-of-more-than-50-which-concepts-will-dominate-the-market, 2023.

[3] D. Stockhouse, M. Phadnis, A. Henry, N. Abbas, M. Sinner, M. Pusch, and L. Y. Pao, "Sink or swim: A tutorial on the control of floating wind turbines," in *2023 American Control Conference (ACC)*, pp. 2512–2529, IEEE, 2023.

[4] J. Meyers, C. Bottasso, K. Dykes, P. Fleming, P. Gebraad, G. Giebel, T. Göçmen, and J. W. van Wingerden, "Wind farm flow control: prospects and challenges," *Wind Energy Science*, vol. 7, no. 6, pp. 2271–2306, 2022.

[5] F. Campagnolo, V. Petrović, C. L. Bottasso, and A. Croce, "Wind tunnel testing of wake control strategies," in *2016 American Control Conference (ACC)*, pp. 513–518, IEEE, 2016.

[6] M. F. Howland, S. K. Lele, and J. O. Dabiri, "Wind farm power optimization through wake steering," *Proceedings of the National Academy of Sciences*, vol. 116, no. 29, pp. 14495–14500, 2019.

[7] M. J. van den Broek, M. Becker, B. Sanderse, and J. W. van Wingerden, "Dynamic wind farm flow control using free-vortex wake models," *Wind Energy Science Discussions*, vol. 2023, pp. 1–28, 2023.

[8] E. M. Nanos, C. L. Bottasso, S. Tamaro, D. I. Manolas, and V. A. Riziotis, "Vertical wake deflection for floating wind turbines by differential ballast control," *Wind Energy Science*, vol. 7, no. 4, pp. 1641–1660, 2022.
[9] W. Munters and J. Meyers, "Towards practical dynamic induction control of wind farms: analysis of optimally controlled wind-farm boundary layers and sinusoidal induction control of first-row turbines," *Wind Energy Science*, vol. 3, pp. 409–425, 2018.
[10] J. A. Frederik, B. M. Doekemeijer, S. P. Mulders, and J. W. van Wingerden, "The helix approach: Using dynamic individual pitch control to enhance wake mixing in wind farms," *Wind Energy*, vol. 23, no. 8, pp. 1739–1751, 2020.
[11] F. Lemmer, W. Yu, P. W. Cheng, A. Pegalajar-Jurado, M. Borg, R. Mikkelsen, and H. Bredmose, "The TripleSpar Campaign: Validation of a Reduced-Order Simulation Model for Floating Wind Turbines," in *Ph.D. Thesis Universität Stuttgart*, 2018.
[12] D. van den Berg, D. De Tavernier, and J. W. van Wingerden, "Using the Helix Mixing Approach on Floating Offshore Wind Turbines," *Journal of Physics: Conference Series*, vol. 2265, p. 042011, 2022.
[13] D. van den Berg, D. De Tavernier, D. Marten, J. Saverin, and J. W. van Wingerden, "Wake Mixing Control for Floating Wind Farms - Analysis of the Implementation of the Helix Wake Mixing Strategy on the IEA 15MW Floating Wind Turbine," *In Publication: Control Systems Magazine*, 2024.
[14] D. Marten, *QBlade: a modern tool for the aeroelastic simulation of wind turbines*. PhD thesis, Technische Universität Berlin, 2020.
[15] F. Papi, G. Troise, R. Behrens de Luna, J. Saverin, S. Perez-Becker, D. Marten, M.-L. Ducasse, and A. Bianchini, "A code-to-code comparison for floating offshore wind turbine simulation in realistic environmental conditions: Quantifying the impact of modeling fidelity on different substructure concepts," *Wind Energy Science Discussions*, vol. 2023, pp. 1–34, 2023.
[16] D. Marten, C. O. Paschereit, X. Huang, M. Meinke, W. Schröder, J. Müller, and K. Oberleithner, "Predicting wind turbine wake breakdown using a free vortex wake code," *AIAA Journal*, vol. 58, pp. 4672–4685, 2020.
[17] D. van den Berg, D. De Tavernier, and J. W. van Wingerden, "The dynamic coupling between the pulse wake mixing strategy and floating wind turbines," *Wind Energy Science*, vol. 8, no. 5, pp. 849–864, 2023.
[18] C. Bak, F. Zahle, R. Bitsche, T. Kim, A. Yde, L. C. Henriksen, M. H. Hansen, J. P. A. A. Blasques, M. Gaunaa, and A. Natarajan, "The DTU 10-MW Reference Wind Turbine," 2013.
[19] V. Arnal, *Experimental modelling of a floating wind turbine using a software-in-the-loop approach*. PhD thesis, École centrale de Nantes, 2020.
[20] G. Lazzerini, D. Coiro, and G. Troise, "Floating Platform and Mooring Lines Optimization for Wake Loss Mitigation in Offshore Wind Farms through Wake Mixing Strategy," *In Publication: IET Renewable Power Generation, Special Issue: Selected Papers from the Offshore Energy Storage Symposium*, 2024.
[21] D. van der Hoek, B. V. den Abbeele, C. Simao Ferreira, and J. W. van Wingerden, "Maximizing wind farm power output with the helix approach: Experimental validation and wake analysis using tomographic particle image velocimetry," *Wind Energy*, pp. 1–20, 2024.
[22] F. V. Mühle, F. M. Heckmeier, F. Campagnolo, and C. Breitsamter, "Wind tunnel investigations of an individual pitch control strategy for wind farm power optimization," *Wind Energy Science Discussions*, vol. 2023, pp. 1–31, 2023.
[23] L. Brandetti and D. van den Berg, "QBlade 2.0.5.2 Matlab Tutorial," 2023.
[24] M. Coquelet, *Numerical investigation of wind turbine control schemes for load alleviation and wake effects mitigation*. PhD thesis, UCL-Université Catholique de Louvain, 2022.
[25] H. Korb, H. Asmuth, and S. Ivanell, "The characteristics of helically deflected wind turbine wakes," *Journal of Fluid Mechanics*, vol. 965, p. A2, 2023.
[26] "IEC 61400-3-1:2019: Wind energy generation systems - Part 3-1: Design requirements for fixed offshore wind turbines," standard, International Electrotechnical Commission, Geneva, CH, 2019.
[27] K. Hasselmann *et al.*, "Measurements of wind-wave growth and swell decay during the Joint North Sea Wave Project (JONSWAP).," *Ergaenzungsheft zur Deutschen Hydrographischen Zeitschrift, Reihe A*, pp. 1–95, 01 1973.
[28] G. Bir, "Multi-Blade Coordinate Transformation and its Application to Wind Turbine Analysis," *46th AIAA Aerospace Sciences Meeting and Exhibit*, 2008.
[29] G. van der Veen, J. W. van Wingerden, M. Bergamasco, M. Lovera, and M. Verhaegen, "Closed-loop subspace identification methods: an overview," *IET Control Theory & Applications*, vol. 7, no. 10, pp. 1339–1358, 2013.
[30] E. Gaertner *et al.*, "IEA wind TCP Task 37: Definition of the IEA 15-Megawatt Offshore Reference Wind Turbine," 3 2020.
[31] D. van den Berg, "Data set containing results used in work. Available at the 4TU repository.." https://doi.org/10.4121/97ce0a99-bdaa-4fbf-b548-f6d85c017915.v2, 2024.